

The Critical Magnetic Field Strength for Suppression of the Richtmyer-Meshkov Instability

Takayoshi Sano,^{1,*} Tsuyoshi Inoue,² and Katsunobu Nishihara¹

¹*Institute of Laser Engineering, Osaka University, Suita, Osaka 565-0871, Japan*

²*Department of Physics and Mathematics, Aoyama Gakuin University, Sagamihara, Kanagawa 252-5258, Japan*

(Dated: April 17, 2019)

The critical strength of a magnetic field required for the suppression of the Richtmyer-Meshkov instability (RMI) is investigated numerically by using a two-dimensional single-mode analysis. For the cases of MHD parallel shocks, the RMI can be stabilized as a result of the extraction of vorticity from the interface. A useful formula describing a critical condition for MHD RMI has been introduced, and which is successfully confirmed by the direct numerical simulations. The critical field strength is found to be largely depending on the Mach number of the incident shock. If the shock is strong enough, even low- β plasmas can be subject to the growth of the RMI.

The Richtmyer-Meshkov instability (RMI) in magneto-hydrodynamics is of great interest in many fields such as astrophysical phenomena, laboratory experiments, and inertial confinement fusion [1, 2]. The RMI occurs when an incident shock strikes a corrugated contact discontinuity [3, 4]. A strong shock wave traveling through the density inhomogeneity of magnetized interstellar medium is a promising site of the RMI. This astrophysically common event plays a key role to determine the dynamics of supernova remnants [5] and gamma ray bursts [6]. Recent laboratory experiments are designed to test the magnetic field amplification due to the RMI by the use of laser-induced shock waves [7]. In inertial confinement fusion, the RMI excited at several capsule interfaces amplifies the perturbations that seed the Rayleigh-Taylor instability. For the fast ignition approach, the utilization of an external magnetic field to guide the fast electrons is discussed proactively, and which shed the light on the impact of MHD instabilities during the implosion [8, 9].

Inclusion of a magnetic field brings two important consequences into the RMI, which are the amplification of an ambient field and the suppression of the unstable motions. The magnetic field can be amplified by the stretching motions at the interface associated with the RMI [10]. Samtaney [11] have shown that a strong magnetic field inhibits the nonlinear turbulent motions of the RMI. The vorticity generated by the interaction between a shock front and a corrugated contact discontinuity is the driving mechanism for the RMI. For the cases of MHD parallel shocks, the role of the magnetic field is to prevent the deposition of the vorticity on the interface, and stabilize the RMI [12, 13].

In the weakest field limit, the RMI should happen just like the hydrodynamical cases, so that there must exist the critical field strength for the suppression. However, how large field is necessary to kill the RMI is still an open question. The previous works are mostly focusing on the weak shock cases. The Mach number of astrophysical and laboratory shocks takes various values including extremely large ones. Thus, the goal of this letter is to

evaluate the critical field strength by studying the evolutions of the RMI systematically in a quite wide range of parameters.

We adopted a single-mode analysis for the MHD RMI in two-dimensions, the same as Sano *et al.* [10] in which the detailed settings and numerical method are described. The initial configuration of the system is illustrated in Fig. 1(a). The contact discontinuity separates two fluids with the densities ρ_1 and $\rho_2 (> \rho_1)$. The corrugation of the contact surface is a key ingredient for the RMI. The interface is assumed to be sinusoidal with a wavelength $\lambda = 2\pi/k$ where k is the wavenumber. Then, the discontinuity is characterized by two parameters; the ratio of the corrugation amplitude to the wavelength ψ_0/λ and the density jump ρ_2/ρ_1 .

The incident shock propagates through the light fluid 1 with a shock velocity U_i and hits the interface at $t = 0$, where V_1 is the fluid velocity behind the shock [see Fig. 1(a)]. The shock strength is indicated by the sonic Mach number $M = |U_i|/c_{s1}$, where $c_{s1} = (\gamma P_0/\rho_1)^{1/2}$ is the sound speed in the fluid 1, γ is the ratio of the specific heats, and P_0 is the initial pressure. When the incident shock hits the corrugated contact discontinuity, the reflected and transmitted shocks start to travel from the interface in the opposite directions with the velocities U_r and U_t , respectively. The RMI can take place in such the situation, and a spike grows linearly with time from the heavy fluid toward the light one.

For the hydrodynamical cases, the asymptotic growth velocity of the RMI can be derived from the linear analysis [14, 15], which is written as

$$v_{\text{lin}} = \frac{\rho_1^* \delta v_1^* - \rho_2^* \delta v_2^*}{\rho_1^* + \rho_2^*}, \quad (1)$$

where ρ_1^* and ρ_2^* are the postshock densities of each fluid, and $\delta v_1^* = k\psi_r(v^* - V_1)$ and $\delta v_2^* = k\psi_t v^*$ are the tangential velocities generated by the refraction of fluid motions at the reflected and transmitted shocks. Here, v^* is the postshock velocity of the interface, and $\psi_r = \psi_0(1 - U_r/U_i)$ and $\psi_t = \psi_0(1 - U_t/U_i)$ are the

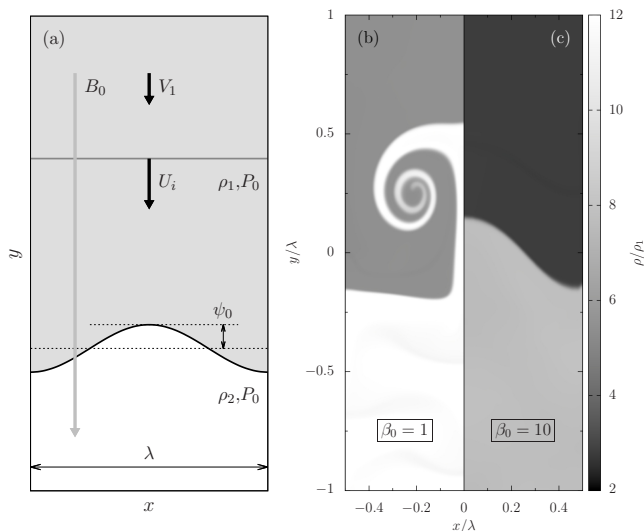


FIG. 1. (a) Sketch of the initial configuration for the single-mode RMI simulations. The sinusoidal corrugation of a contact discontinuity is given by $y = \psi_0 \cos(kx)$ and an incident shock moves in the y direction with the velocity $U_i (< 0)$. (b,c) Numerical results of the RMI for the models with (b) a stronger field $\beta_0 = 1$ and (c) a weaker field $\beta_0 = 10$. The gray color denotes the density profiles at the later evolutionary stage of the RMI taken at $kv_{\text{lin}}t = 10$. For the both models, the initial corrugation amplitude is $\psi_0/\lambda = 0.1$ and the initial density jump is $\rho_2/\rho_1 = 3$. The Mach number of the incident shock is (b) $M = 200$ and (c) $M = 2$.

initial ripple amplitudes of each shock. The Atwood number of the postshocked interface can be defined by $A^* = (\rho_2^* - \rho_1^*)/(\rho_2^* + \rho_1^*)$. The growth velocity v_{lin} given by Eq. (1) is an exact solution in the weak shock limit. When the Mach number is large, the bulk vorticity left behind the rippled transmitted shock reduces v_{lin} by a factor of a few [15]. The MHD effects could also modify the growth velocity [12, 13]. However, as with our previous analysis [10], we adopt Equation (1) for the typical growth velocity.

In this letter, only the parallel shock cases are considered, so that a uniform magnetic field perpendicular to the shock surface, $(B_x, B_y) = (0, B_0)$, is assumed. The initial field strength is given by the plasma beta $\beta_0 = 8\pi P_0/B_0^2$ in the preshocked regions. We solve the ideal MHD equations, and most of the calculations use a grid resolution of $\Delta_x = \Delta_y = \lambda/256$ unless otherwise stated.

Figures 1(b) and 1(c) show the simulation results of the density distribution at the later stage of the RMI ($kv_{\text{lin}}t = 10$) for two different models. The mushroom-shaped spike and roll-up due to the growth of the RMI can be seen in Fig. 1(b), while the corrugation amplitude does not change by much for the model in Fig. 1(c). The plasma beta is initially $\beta_0 = 1$ and 10 for the models in Figs. 1(b) and 1(c), respectively, and then the field strength is stronger in the unstable model and weaker in

the stabilized model.

Interestingly, even when the preshocked plasma is strongly magnetized as $\beta_0 = 1$, the RMI is not necessarily suppressed. Reversely, there exists a case that the RMI is quenched completely by a weaker field with $\beta_0 = 10$. These results clearly demonstrate that the critical field strength cannot be simply described as $\beta \sim 1$. Then, what determines the conditions for suppression of the RMI?

It is found that the Mach number of the incident shock has a huge impact on the critical field strength. For the both models in Fig. 1, the parameters related to the contact discontinuity are identical, that is, $\psi_0/\lambda = 0.1$ and $\rho_2/\rho_1 = 3$. But, the Mach number is $M = 200$ and 2 in Figs. 1(b) and 1(c), respectively, which indicates that the weaker shock case could be stabilized by a much weaker field.

Wheatley *et al.* [13] have found that the presence of a magnetic field affects the refraction of fluid motions at the reflected and transmitted shocks. For the cases of MHD, each shock could split into a combination of the waves and/or discontinuities associated with the fast, Alfvén, and slow modes. In contrast to hydrodynamical shocks, the jump in the tangential velocity can exist only at the MHD waves, and is not allowed to be at the contact discontinuity.

Let us consider the conservation laws related to the momentum and the tangential electric field component in the discontinuity frame [16];

$$\left[\rho v_n v_t - \frac{B_n B_t}{4\pi} \right] = 0, \quad (2)$$

$$[v_n B_t - v_t B_n] = 0, \quad (3)$$

where the square brackets mean the difference between the values on the two sides of the discontinuity. The subscript n and t denote the normal and transverse components, respectively. For the contact discontinuity, the normal velocity is $v_n = 0$, so that it should be satisfied that $[v_t] = [B_t] = 0$ when $B_n \neq 0$. Therefore, the vortex sheet and the current sheet cannot be located at the contact discontinuity. Although the vorticity is generated instantaneously at the interface, it must move away from the interface with the MHD waves. This feature could affect seriously on the nonlinear evolutions of the MHD RMI.

Figures 2(a) and 2(b) show the zoomed-in views of spatial distributions for the density, field lines, and vorticity. The snapshot data are taken just after the interaction at $kv_{\text{lin}}t = 0.2$. These figures are to demonstrate the comparison between a weak field case $\beta_0 = 100$ [Fig. 2(a)] and a strong field case $\beta_0 = 0.1$ [Fig. 2(b)]. All the model parameters other than β_0 are identical, which are $M = 20$, $\psi_0/\lambda = 0.1$, and $\rho_2/\rho_1 = 3$.

Three discontinuous surfaces can be recognized easily from the density contrast, which are interpreted as the reflected fast shock, contact discontinuity, and transmitted

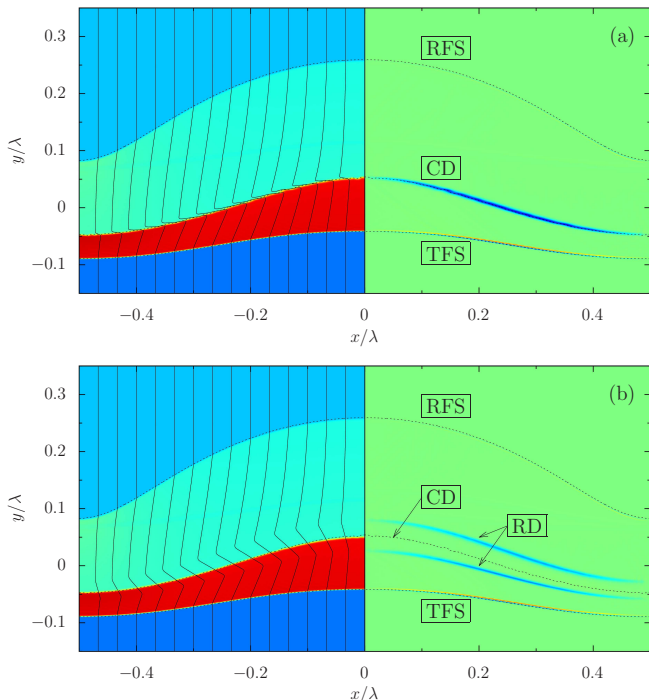


FIG. 2. (a) Spatial distributions of the density (left panel) and the vorticity (right panel) near the contact discontinuity. These snapshots are taken just after the interaction with the incident shock at $kv_{\text{lin}}t = 0.2$. The magnetic field lines are also depicted over the density profile. The dotted curves denote the surfaces of the reflected fast shock (RFS), contact discontinuity (CD), and transmitted fast shock (TFS), from top to bottom. The model parameters are $M = 20$, $\psi_0/\lambda = 0.1$, $\rho_2/\rho_1 = 3$, and $\beta_0 = 100$. The higher resolution $\Delta_x = \Delta_y = \lambda/1024$ is used for this figure. (b) The same figure for a model with a stronger initial field with $\beta_0 = 0.1$. The other parameters are identical to the model in (a). The rotational discontinuities (RD) appear at the both sides of the CD for this case.

fast shock. At this early stage, the density distributions are almost the same in the both cases. However, obvious differences have appeared later at the nonlinear regime of the RMI.

In fact, significant growth of a spike due to the RMI can be seen only in the weak field case. For this case, the shape of the vortex sheet always evolves together with the contact surface throughout the calculation. Despite of a serious kink of the field lines near the contact discontinuity, the weak field cannot influence the fluid motions and vorticity distribution. Therefore, the RMI grows nonlinearly in a similar manner as the hydrodynamical cases.

For the strong field case, on the other hand, the vorticity is no longer associated with the contact discontinuity and split into two oppositely propagating sheets. For this case, another discontinuity in between the fast shock and contact surface can be identified by a kink of the field lines as well as the location of the vortex sheet. Because the density is continuous and the direction of

the tangential field is opposite across this discontinuity, the structure coincides with the rotational discontinuity. The propagation velocity of the rotational discontinuity corresponds to the Alfvén speed, and the extraction of the vorticity leads to the suppression of the RMI.

Even for the weak field case, the vortex sheet should be propagating with the Alfvén speed. However, it would be too slow to make a difference in the evolutions of the RMI. For the model shown in Fig. 2(a), the ratio of the Alfvén speed to the growth velocity is much smaller than unity. When the Alfvén speed becomes comparable to v_{lin} given by Eq. (1), then the growth of the RMI seems to be severely reduced. It is inferred from this fact that the competition between the Alfvén speed and v_{lin} could be a controlling factor of the MHD RMI.

Here we introduce a condition that the Alfvén speed exceeds the growth velocity of the RMI,

$$v_{A2}^* \gtrsim \alpha v_{\text{lin}}, \quad (4)$$

where the Alfvén speed is represented by $v_{A2}^* = B_0/(4\pi\rho_2^*)^{1/2}$ estimated in the heavy fluid 2. The growth velocity at the nonlinear regime is assumed to be αv_{lin} where α is typically of the order of 0.1 based on the direct numerical simulations [10, 17].

Then, the critical field strength $B_{\text{crit}} \equiv (4\pi\rho_2^*)^{1/2}\alpha v_{\text{lin}}$ can be expressed in terms of β as

$$\beta_{\text{crit}} \equiv \frac{8\pi P_0}{B_{\text{crit}}^2} = \frac{2}{\gamma} \alpha^{-2} \left(\frac{v_{\text{lin}}}{c_{s2}^*} \right)^{-2} \left(\frac{P^*}{P_0} \right)^{-1}, \quad (5)$$

where $c_{s2}^* \equiv (\gamma P^*/\rho_2^*)^{1/2}$ is the postshock sound speed in the spike, and P^* is the postshock pressure at the interface. The critical β given by Eq. (5) can be evaluated by solving a Riemann problem relevant to a set of the initial parameters M and ρ_2/ρ_1 . Notice that β_{crit} is defined by the preshock pressure P_0 .

The growth velocity v_{lin} is roughly proportional to the incident shock velocity U_i , or the Mach number M . Then the critical strength B_{crit} will be proportional to M , because the postshock density ρ_2^* is almost constant in the strong shock limit. The sound speed c_{s2}^* in Eq. (5) is typically comparable to or an order of magnitude smaller than v_{lin} . The ratio c_{s2}^*/v_{lin} has little dependence on the model parameters, and then the size of β_{crit} is determined by the amplification factor of the pressure P^*/P_0 .

In Fig. 3(a), the critical field strength is shown by the solid curve as a function of the Mach number M . As for the fiducial case, we choose $\psi_0/\lambda = 0.1$ and $\rho_2/\rho_1 = 3$. As expected, the critical β decreases dramatically as M increases. This condition suggests that, for the strong shock cases ($M \gtrsim 30$), the RMI could occur under a very strong ambient field as $\beta_0 \lesssim 1$. But if the shock is weak ($M \lesssim 3$), then the RMI will be suppressed even by a weaker field of $\beta_0 \gtrsim 100$.

In order to confirm the validity of this criterion, we performed the direct numerical simulations of the RMI

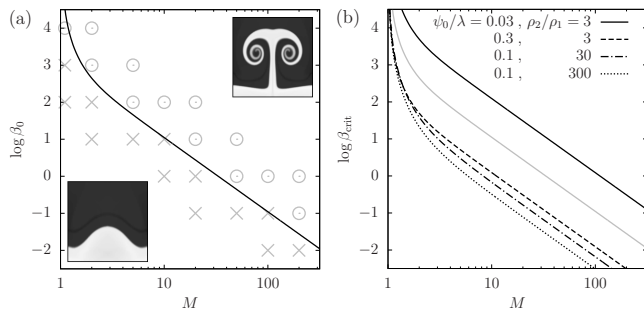


FIG. 3. (a) The critical field strength as a function of the Mach number of the incident shock. The solid curve is for the fiducial case with $\psi_0/\lambda = 0.1$ and $\rho_2/\rho_1 = 3$. The circles denote the unstable models that exhibit the nonlinear growth of RMI in the numerical simulations, whereas the crosses stand for the models which are stabilized by the ambient magnetic field. Insets are typical results for the shape of the interface at $kv_{\text{lin}}t = 10$ in an unstable model with $\beta_0 = 100$ and $M = 20$ (top panel), and in a stabilized model with $\beta_0 = 0.1$ and $M = 20$ (bottom panel). (b) The critical field strength estimated from Eq. (5) for various set of parameters ψ_0/λ and ρ_2/ρ_1 . The parameter space above the critical curve corresponds to the unstable regions for the MHD RMI. For comparison, the critical curve for the fiducial case ($\psi_0/\lambda = 0.1$ and $\rho_2/\rho_1 = 3$) is also shown by the gray curve.

for various sets of parameters for M , ψ_0/λ , ρ_2/ρ_1 , and β_0 . Nonlinear outcomes of the RMI in each model are depicted by the gray marks in Fig. 3(a). The circles in this figure denote the models in which the nonlinear growth of the RMI can be seen. We define this condition that the growth velocity of the spike continues to take positive values until at least $kv_{\text{lin}}t = 10$. Actually, this is almost equivalent to the condition that the magnetic field is amplified more than 10 times compared to the initial value B_0 by this timescale ($kv_{\text{lin}}t = 10$). The crosses, on the other hand, stand for the models where the RMI is stabilized due to the existence of a magnetic field. In those models, neither the growth of mushroom-shaped spike nor the field amplification can be realized. As seen from Fig. 3(a), the criterion given by Eq. (5) is predicting the nonlinear results of the numerical simulations with fairly good accuracy.

The dependence of the critical β on the other parameters is shown by Fig. 3(b). When the corrugation amplitude is larger (smaller), the growth velocity becomes faster (slower). Then the critical curve shifts downward (upward) in the M - β diagram. The larger density jump at the contact surface causes faster growth of the RMI. For the cases of $\rho_2/\rho_1 = 300$, the critical β becomes 2 orders of magnitude smaller than that for $\rho_2/\rho_1 = 3$. All the critical curves in Fig. 3(b) are reasonably consistent with the simulation results, so that the criterion given by Eq. (5) can be applicable for various situations of the RMI.

The transverse field component B_x also has the sta-

bilizing effect for the RMI through the Lorentz force [18]. Our numerical simulations reveal that the critical strength B_{crit} for the perpendicular shock cases is quantitatively similar to that for the parallel shock cases. We have checked the convergence of the numerical results with respect to the grid resolution. The nonlinear behaviors of the RMI shown in Fig 3(a) are unchanged even with the quarter resolution $\Delta = \lambda/64$ and the quadruple resolution $\Delta = \lambda/1024$.

In summary, we have derived a formula of the critical field strength for suppression of the RMI. The obtained criterion is quite useful for the estimation of the MHD effects on the RMI. For the weak shock cases, for example, a weak field that is dynamically unimportant as $\beta_0 \gg 1$ can reduce the growth of the RMI significantly. When the incident shock is strong enough, on the other hand, nonlinear growth of the RMI is allowed even when the initial plasma β is less than unity. Notice that the high Mach number $M \gg 10$ is characteristics of the interstellar shocks driven by supernova explosions. For those cases, significant growth of the RMI can be expected even when the preshocked gas is strongly magnetized as $\beta_0 \sim 1$. Then the magnetic field can be amplified locally near the interface up to the order of the turbulent energy $B_{\text{max}}^2 \sim \rho v_{\text{lin}}^2$ [10]. This amplification mechanism could explain the origin of the milligauss field observed at young supernova remnants [19].

The linear impulsive model for the MHD RMI [12] shows that the asymptotic amplitude of the interface tends to be $\psi_\infty \approx \psi_0(1 + V/v_{A2}^*)$ when $\rho_2^* > \rho_1^*$, where V is the initial velocity of the impulsively accelerated interface. Therefore, the suppression condition can be expressed as $V/v_{A2}^* \ll 1$, which is qualitatively consistent with our criterion. The growth velocity at the nonlinear regime is assumed empirically as $0.1v_{\text{lin}}$ in this analysis. Obviously the quantitative improvement of the criterion will be an important next step. Furthermore, the extension to three-dimensions is inevitable for the studies of RMI [20]. When the initial field direction is purely in the z -direction, the RMI can always grow independent of the field strength within the two-dimensional approximation [21]. This feature should cause the asymmetric evolutions of MHD RMI, and thus the three-dimensional analysis will be also an interesting subject for our future work.

Computations were carried out on SX-8R at the Cybermedia Center and SX-9/B at the Institute of Laser Engineering of Osaka University. This research work is partly supported by results of HPCI Systems Research Projects (Project ID hp120227).

* sano@ile.osaka-u.ac.jp

[1] M. Brouillette, Annu. Rev. Fluid Mech. **34**, 445 (2002).

- [2] K. Nishihara, J. G. Wouchuk, C. Matsuoka, R. Ishizaki, and V. V. Zhakhovsky, *Phil. Trans. R. Soc. A* **368**, 1769 (2010).
- [3] R. D. Richtmyer, *Commun. Pure Appl. Math.* **13**, 297 (1960).
- [4] E. E. Meshkov, *Fluid Dyn.* **4**, 101 (1969).
- [5] T. Inoue, R. Yamazaki, S. Inutsuka, and Y. Fukui, *Astrophys. J.* **744**, 71 (2012).
- [6] T. Inoue, K. Asano, and K. Ioka, *Astrophys. J.* **734**, 77 (2011).
- [7] Y. Kuramitsu, Y. Sakawa, T. Morita, S. Dono, H. Aoki, H. Tanji, C. D. Gregory, J. N. Waugh, B. Loupias, M. Koenig, N. Woolsey, T. Ide, T. Sano, and H. Takabe, *Astrophys. Space Sci.* **336**, 269 (2011).
- [8] P. Y. Chang, G. Fiksel, M. Hohenberger, J. P. Knauer, R. Betti, F. J. Marshall, D. D. Meyerhofer, F. H. Séguin, and R. D. Petrasso, *Phys. Rev. Lett.* **107**, 035006 (2011).
- [9] D. J. Strozzi, M. Tabak, D. J. Larson, L. Divol, A. J. Kemp, C. Bellei, M. M. Marinak, and M. H. Key, *Phys. Plasmas* **19**, 072711 (2012).
- [10] T. Sano, K. Nishihara, C. Matsuoka, and T. Inoue, *Astrophys. J.* **758**, 126 (2012).
- [11] R. Samtaney, *Phys. Fluids* **15**, L53 (2003).
- [12] V. Wheatley, D. I. Pullin, and R. Samtaney, *Phys. Rev. Lett.* **95**, 125002 (2005).
- [13] V. Wheatley, R. Samtaney, and D. I. Pullin, *Phys. Fluids* **21**, 082102 (2009).
- [14] J. G. Wouchuk and K. Nishihara, *Phys. Plasmas* **3**, 3761 (1996).
- [15] J. G. Wouchuk and K. Nishihara, *Phys. Plasmas* **4**, 1028 (1997).
- [16] L. D. Landau and E. M. Lifshitz, *Electrodynamics of Continuous Media* (Pergamon, Oxford, 1960).
- [17] G. Dimonte and P. Ramaprabhu, *Phys. Fluids* **22**, 014104 (2010).
- [18] J. Cao, Z. Wu, H. Ren, and D. Li, *Phys. Plasmas* **15**, 042102 (2008).
- [19] Y. Uchiyama, F. A. Aharonian, T. Tanaka, T. Takahashi, and Y. Maeda, *Nature (London)* **449**, 576 (2007).
- [20] C. C. Long, V. V. Krivets, J. A. Greenough, and J. W. Jacobs, *Phys. Fluids* **21**, 114104 (2009).
- [21] T. Inoue, *Astrophys. J.* **760**, 43 (2012).